Supporting Information

B-site Cation Sequencing in $SrMnO_3$ Using Iron for Zinc-Air Battery Electrocatalysis: A Structural Evaluation

E. Carolin Mercy[a], Sagar Ingavale[b], Prabakaran Varathan[c,d], Akhila Kumar Sahu[c,d], Anita Swami[a]*

[a] Department of Chemistry, SRM Institute of Science and Technology, Kattankulathur-603203, Chennai (India)

[b]Department of Chemical Engineering, Faculty of Engineering, Chulalongkorn University, Bangkok 10330, Thailand

[c]CSIR - Central Electrochemical Research Institute - Madras Unit, CSIR Madras Complex, Taramani, Chennai - 600 113, India.

[d]Academy of Scientific and Innovative Research (AcSIR), Ghaziabad - 201002, India

*Corresponding author e-mail: swamians@srmist.edu.in, swami.anita@gmail.com

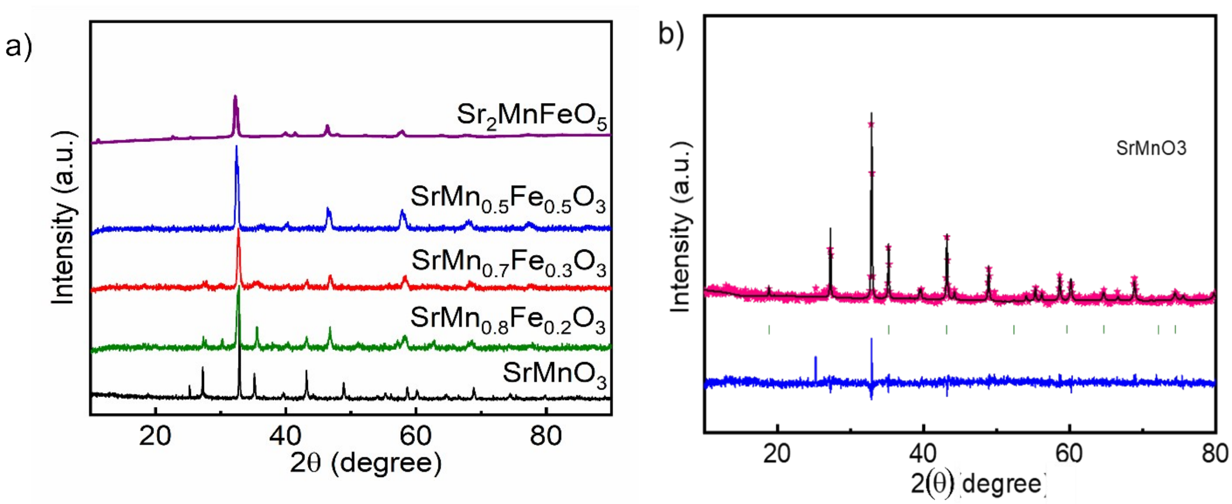

Figure S1: (a) Powder XRD patterns of $SrMnO_3$, $SrMn_{0.8}Fe_{0.2}O_3$, $SrMn_{0.7}Fe_{0.3}O_3$, $SrMn_{0.5}Fe_{0.5}O_3$ Sr_2MnFeO_5 (b) Rietveld refinement of powdered XRD pattern of $SrMnO_3$. The pink stars and black line show the observed and calculated profile respectively, the green vertical lines represent the Bragg diffraction positions, and the blue line shows the difference between the observed profile and the calculated profile.

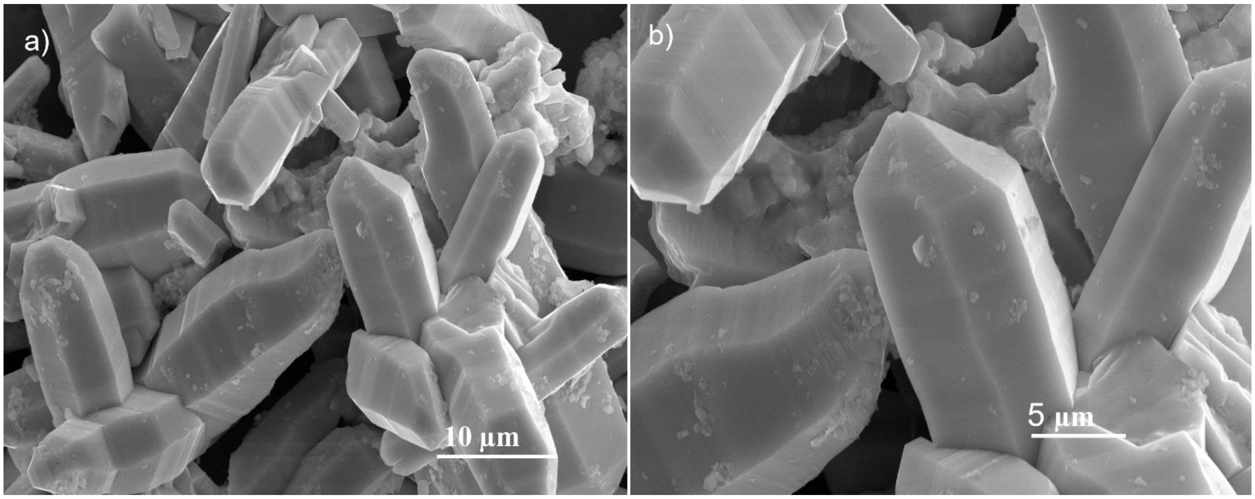

Figure S2: (a-b) SEM images of $SrMnO_3$ [50]

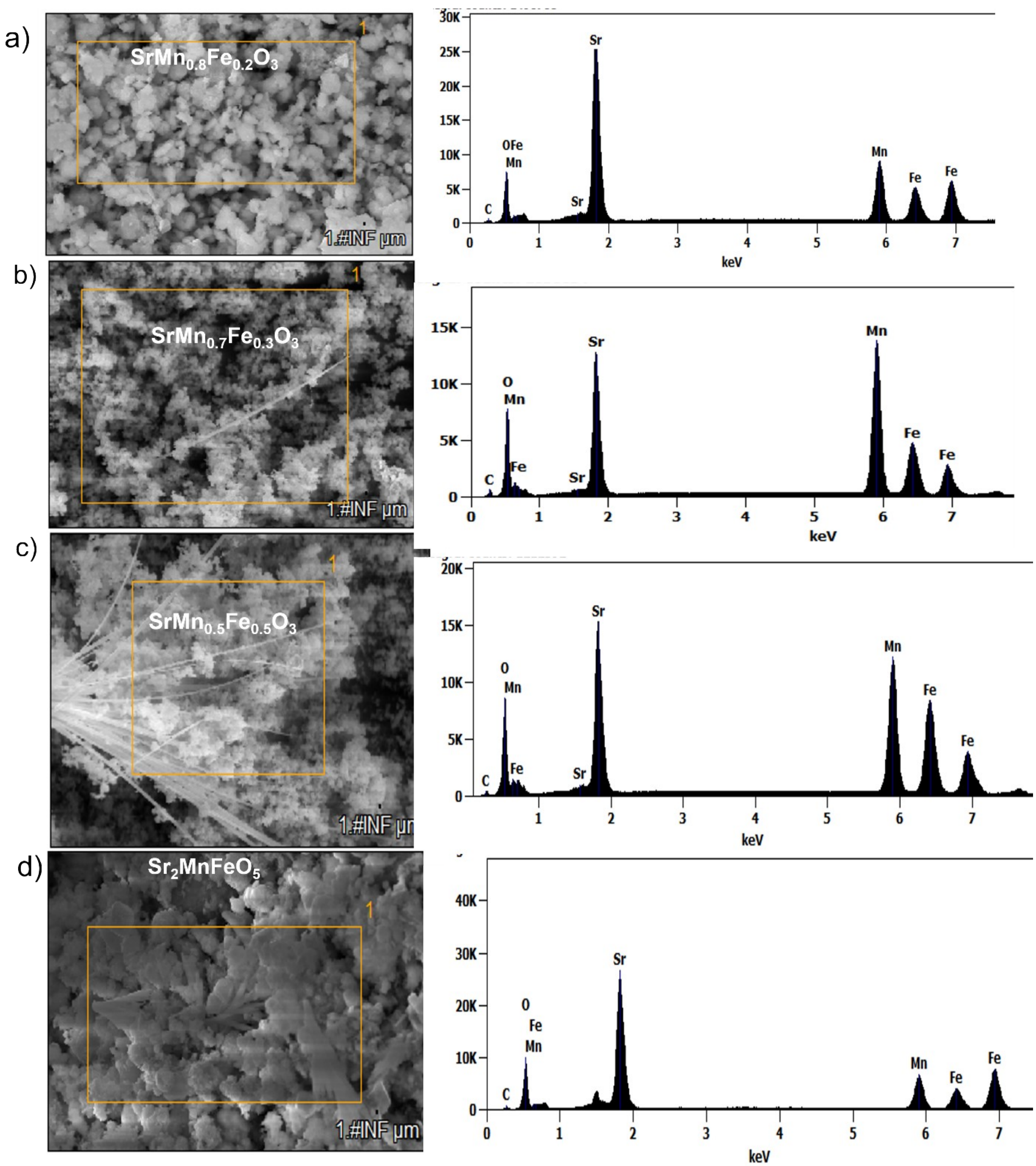

Figure S3: EDX spectra of $SrMn_{0.8}Fe_{0.2}O_3$, $SrMn_{0.7}Fe_{0.3}O_3$, $SrMn_{0.5}Fe_{0.5}O_3$ & Sr_2MnFeO_5

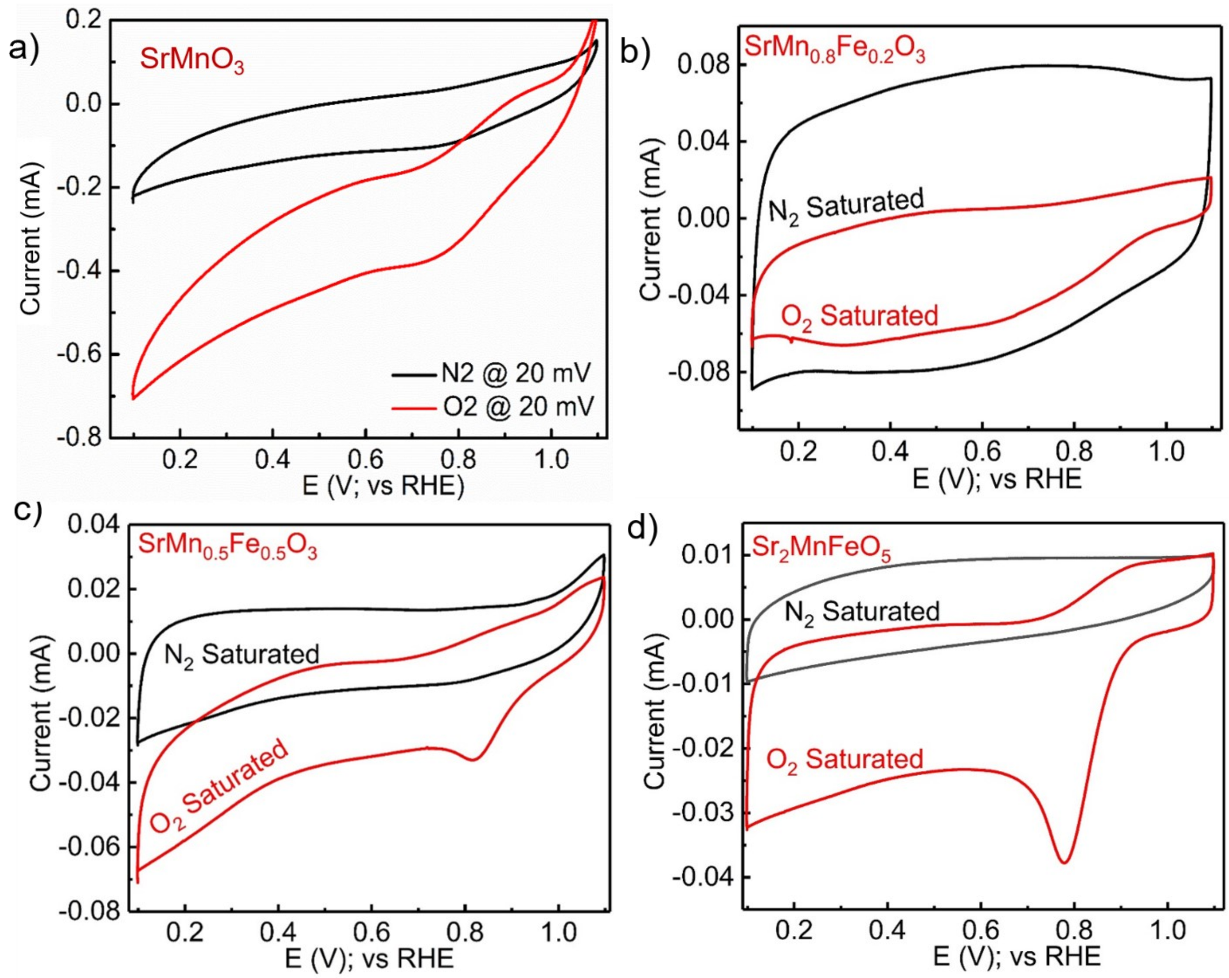

Figure S4: Cyclic voltammograms recorded in N_2 saturated and O_2 saturated 0.1M KOH at 20 mV s^{-1} for (a) $SrMnO_3$, (b) $SrMn_{0.8}Fe_{0.2}O_3$, (c) $SrMn_{0.5}Fe_{0.5}O_3$ and (d) Sr_2MnFeO_5

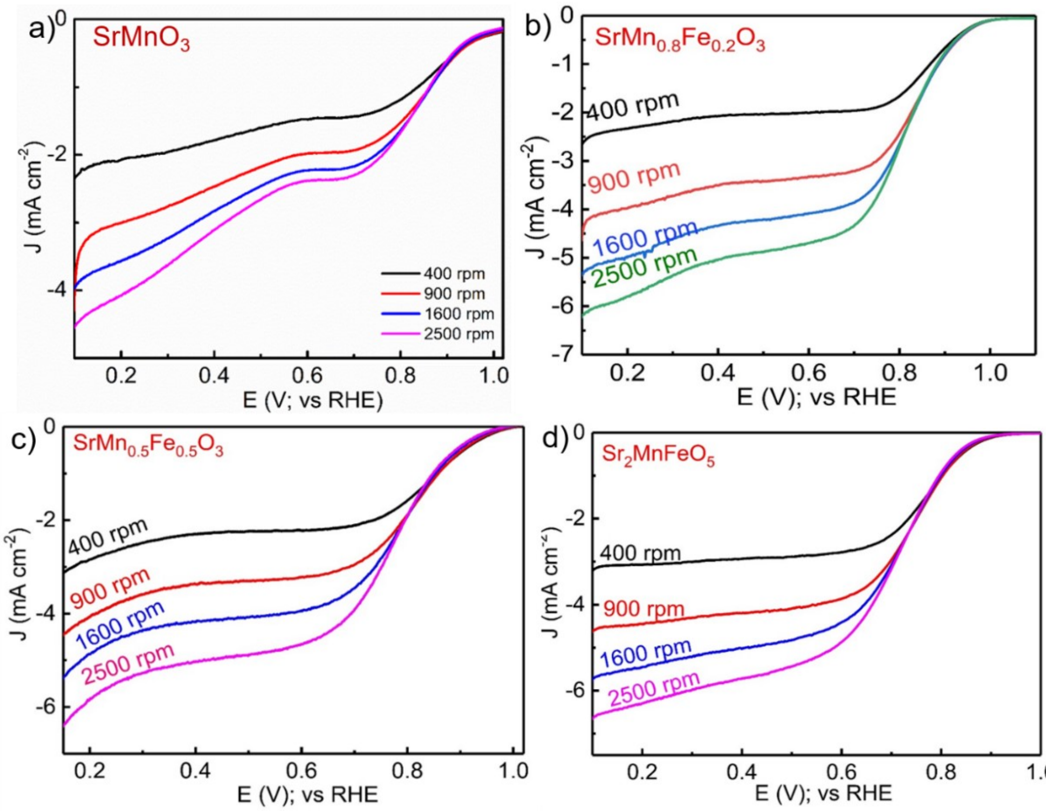

Figure S5: Linear sweep voltammograms of (a) $SrMnO_3$, (b) $SrMn_{0.8}Fe_{0.2}O_3$, (c) $SrMn_{0.5}Fe_{0.5}O_3$ and (d) Sr_2MnFeO_5 recorded at different rotations in O_2 saturated in 0.1M KOH with the scan rate of 10 mVs^{-1}**.**

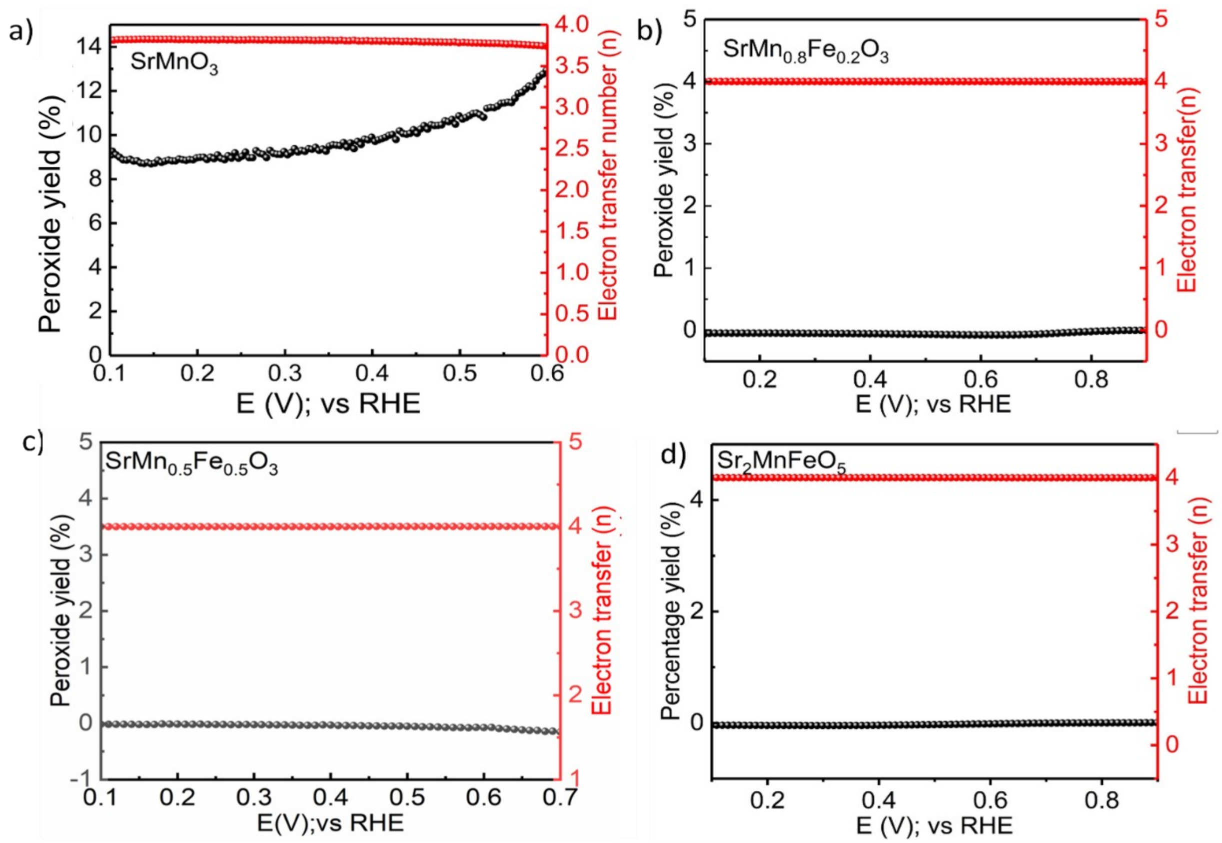

Figure S6: RRDE measurement representing the percentage of hydrogen peroxide and the number of electron transfer under O_2 saturated 0.1 M KOH at 1600 rpm for (a) $SrMnO_3$, (b) $SrMn_{0.8}Fe_{0.2}O_3$, (c) $SrMn_{0.5}Fe_{0.5}O_3$, d) Sr_2MnFeO_5.

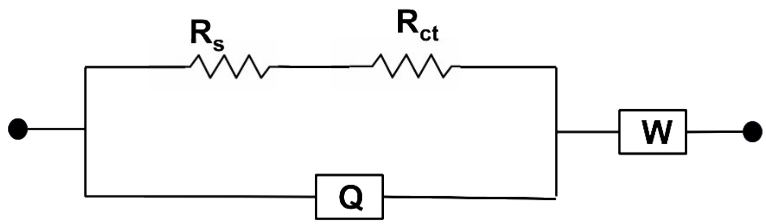

Figure S7: Randles equivalent circuit used for fitting the Nyquist plot of $SrMn_{0.7}Fe_{0.3}O_3$ sample, where R_{ct} represents charge transfer resistance, R_s represents solution resistance and Q represents constant phase element while W represents Warburg impedance.

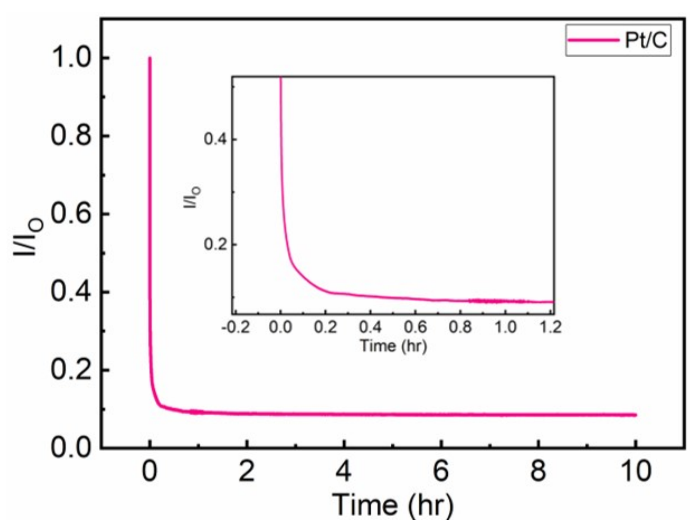

Figure S8: Chronoamperometric measurement for commercial Pt/C catalyst at 0.6 V; vs RHE for 10 hours.

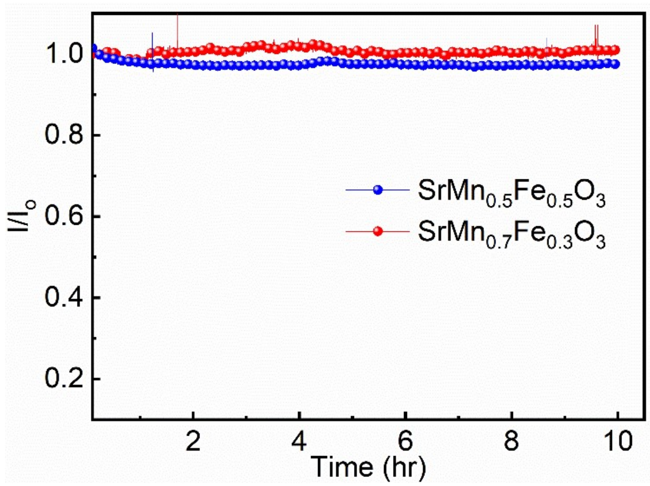

Figure S9: Chronoamperometric measurements of the OER at a current density of 10 mA cm^{-2} for $SrMn_{0.7}Fe_{0.3}O_3$ and $SrMn_{0.5}Fe_{0.5}O_3$

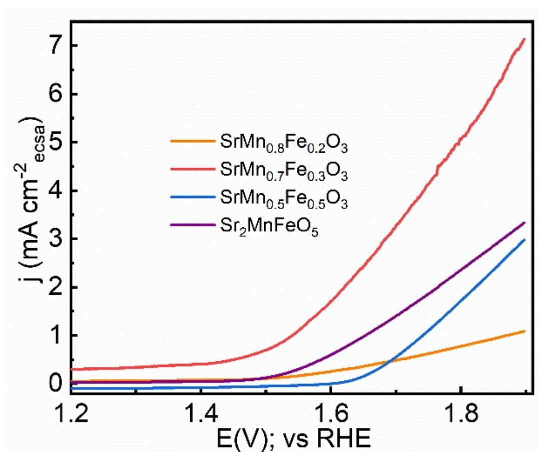

Figure S10: ECSA normalised LSV curves for OER with all the catalysts

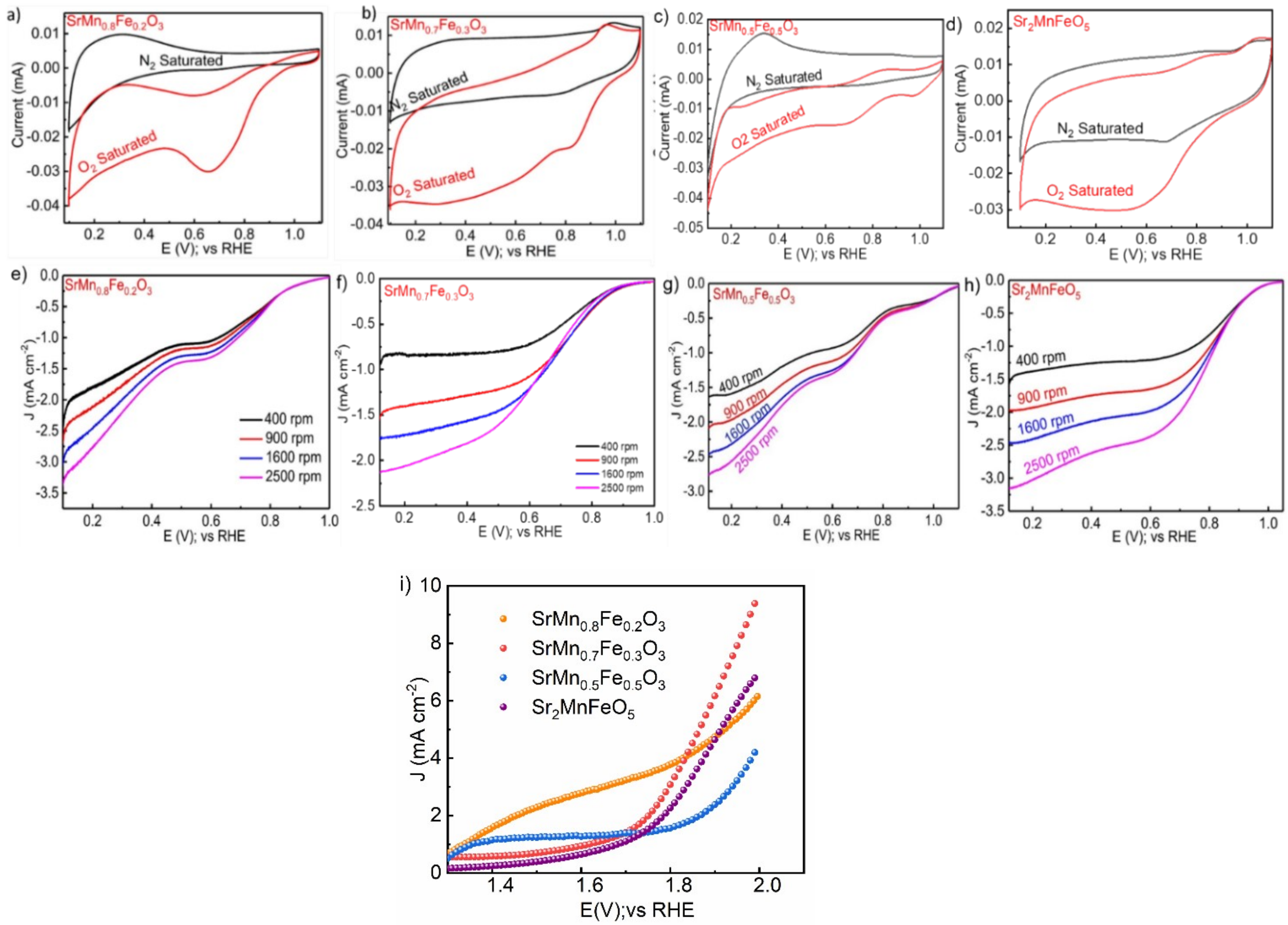

Figure S11: **(**a-h) Cyclic voltammograms of $SrMn_{0.8}Fe_{0.2}O_3$, $SrMn_{0.7}Fe_{0.3}O_3$, $SrMn_{0.5}Fe_{0.5}O_3$, Sr_2MnFeO_5 under N_2 saturated and O_2 saturated 0.1 M KOH and linear sweep voltammograms of $SrMn_{0.8}Fe_{0.2}O_3$, $SrMn_{0.7}Fe_{0.3}O_3$, $SrMn_{0.5}Fe_{0.5}O_3$ and Sr_2MnFeO_5**,** at different rotation in O_2 saturated 0.1M KOH**.** **(**i) Comparative linear sweep voltammograms for OER in 0.1 M KOH under O_2 saturation at 1600 rpm; of all the prepared compounds without carbon support

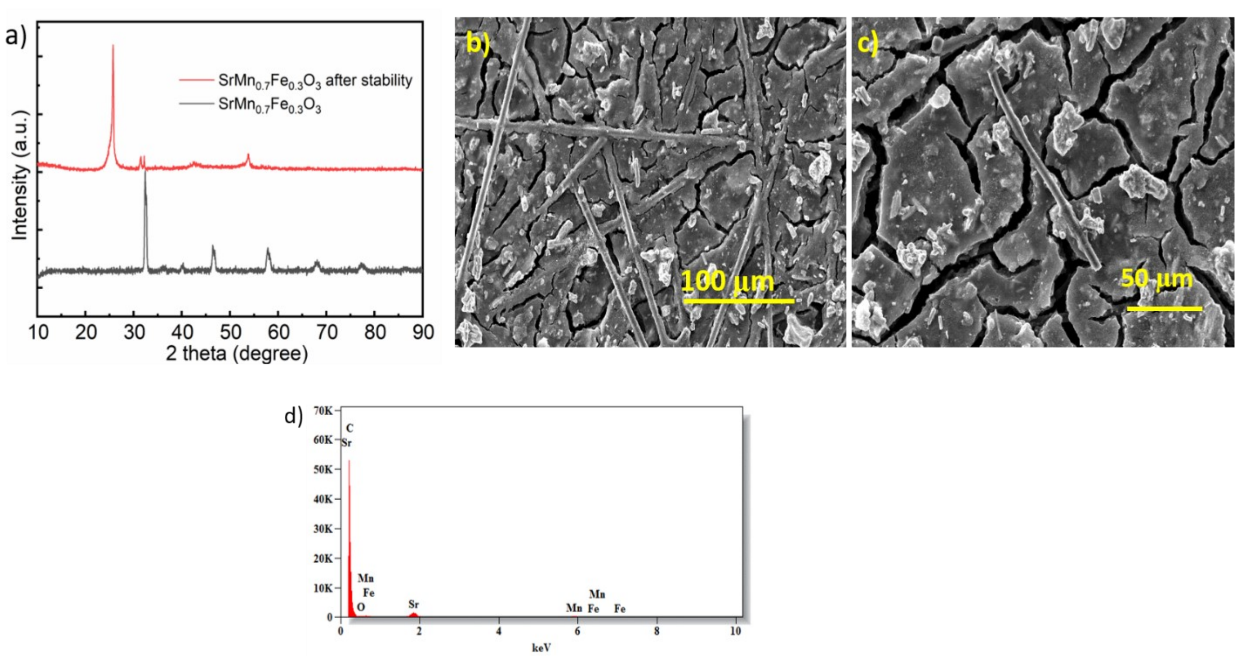

Figure S12: Post stability measurement of $SrMn_{0.7}Fe_{0.3}O_3$: (a)XRD pattern and (b-c)SEM images (d)EDX profile

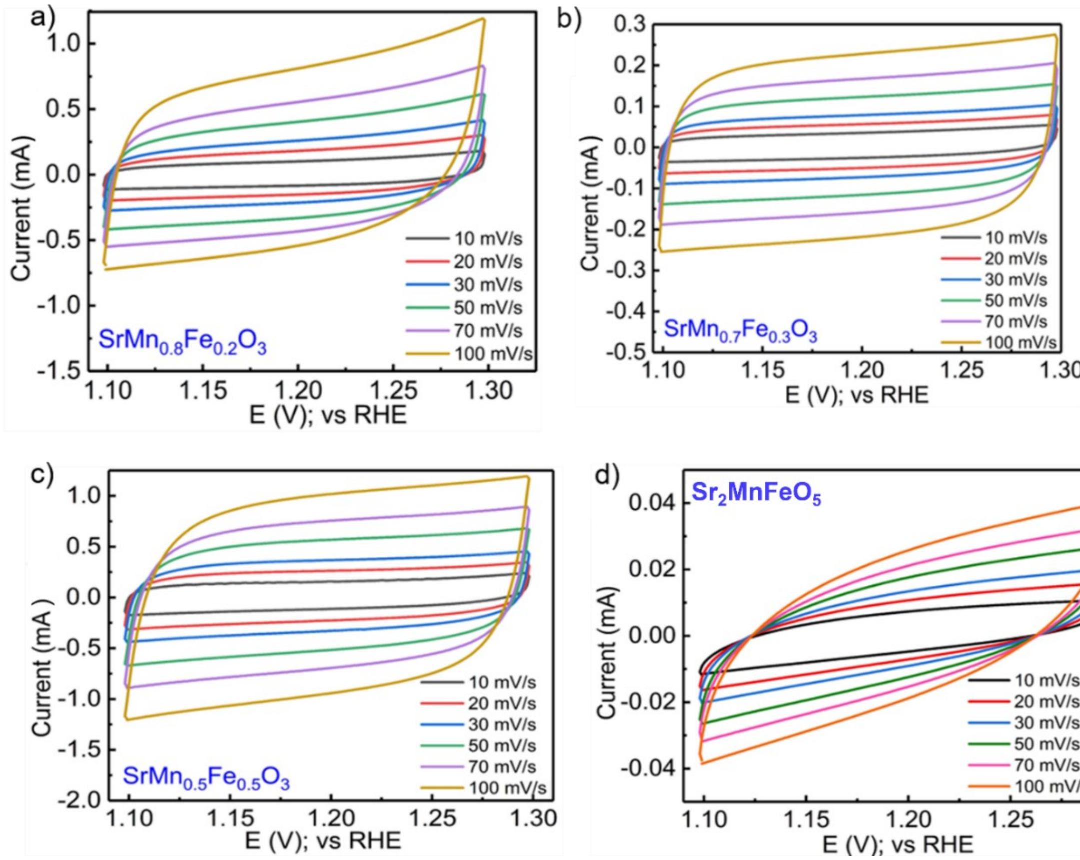

Figure S13: Cyclic voltammograms recorded at different scan rates for all the catalysts loaded on carbon

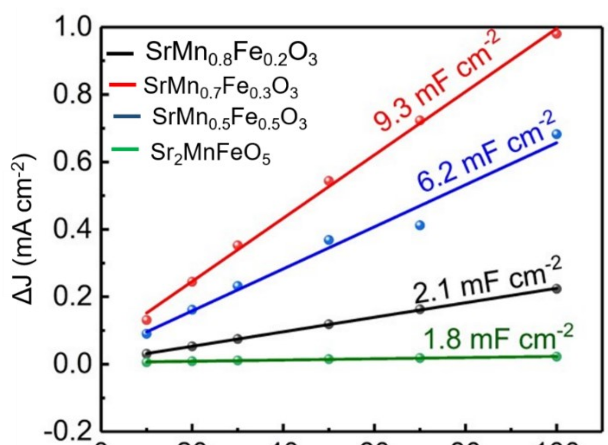

Figure S14: Current densities ($J = J_{anode} - J_{cathode}$) as a function of scan rate plotted for all prepared compounds with a slope proportional to C_{dl} values.

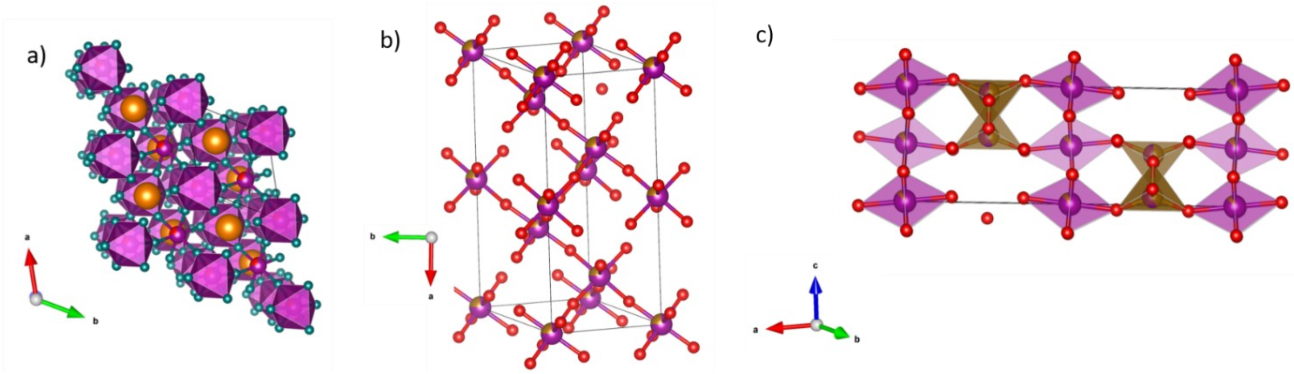

Figure S15: Structural model of (a-b) $SrMn_{0.7}Fe_{0.3}O_3$ perovskite oxide and (c) Sr_2MnFeO_5 [Orange ball represents Strontium; red ball represents iron; purple ball represents manganese and cyan green ball represent oxygen]

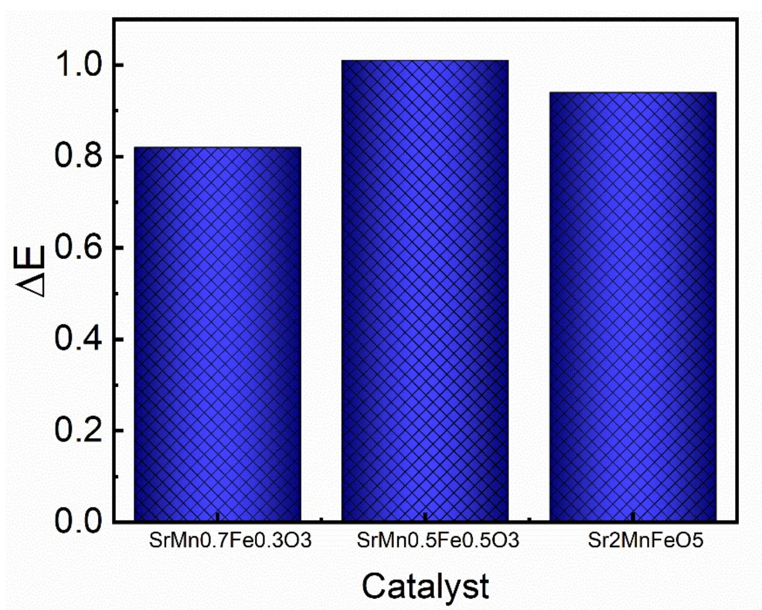

Figure S16: Bifunctionality index of all the catalysts

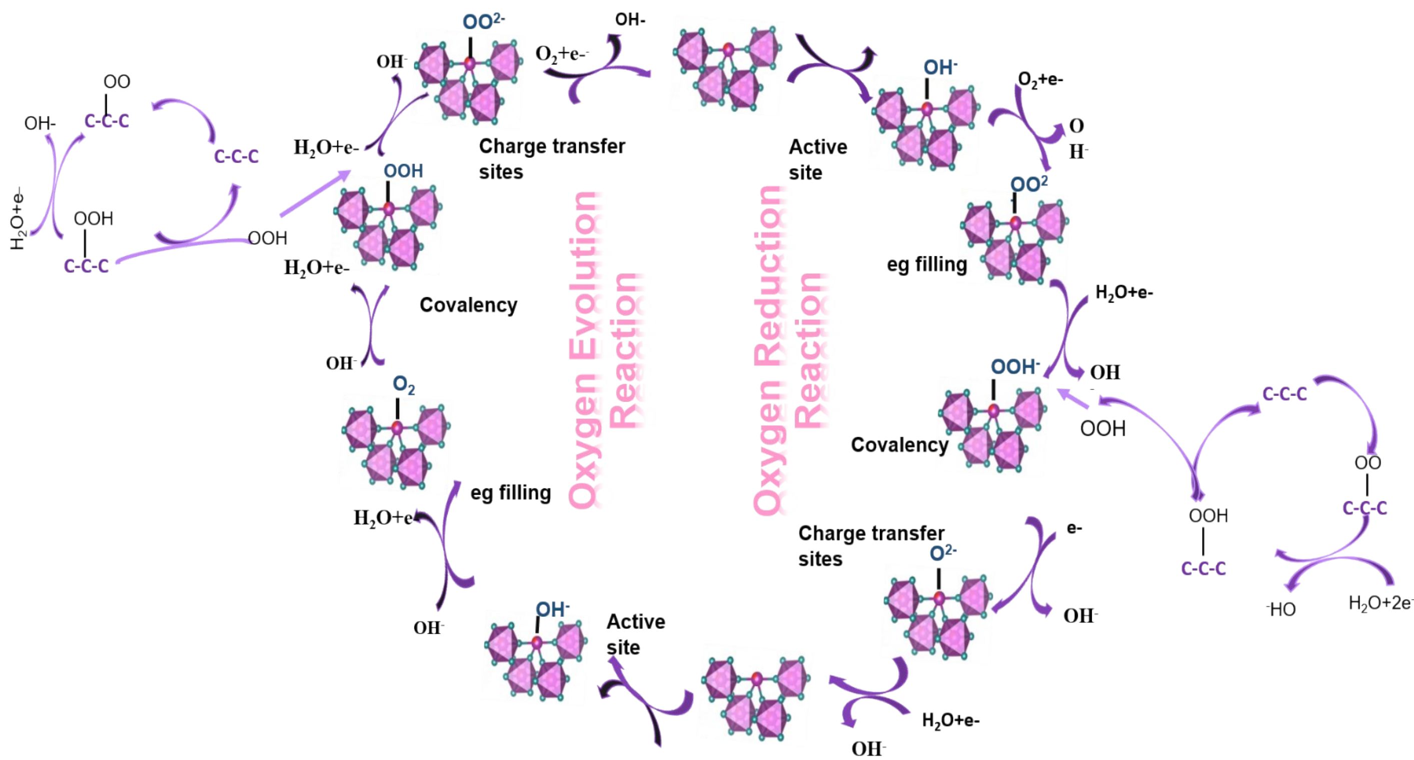

Figure S17: A possible bifunctional mechanism for $SrMn_{0.7}Fe_{0.3}O_3$ perovskite oxide

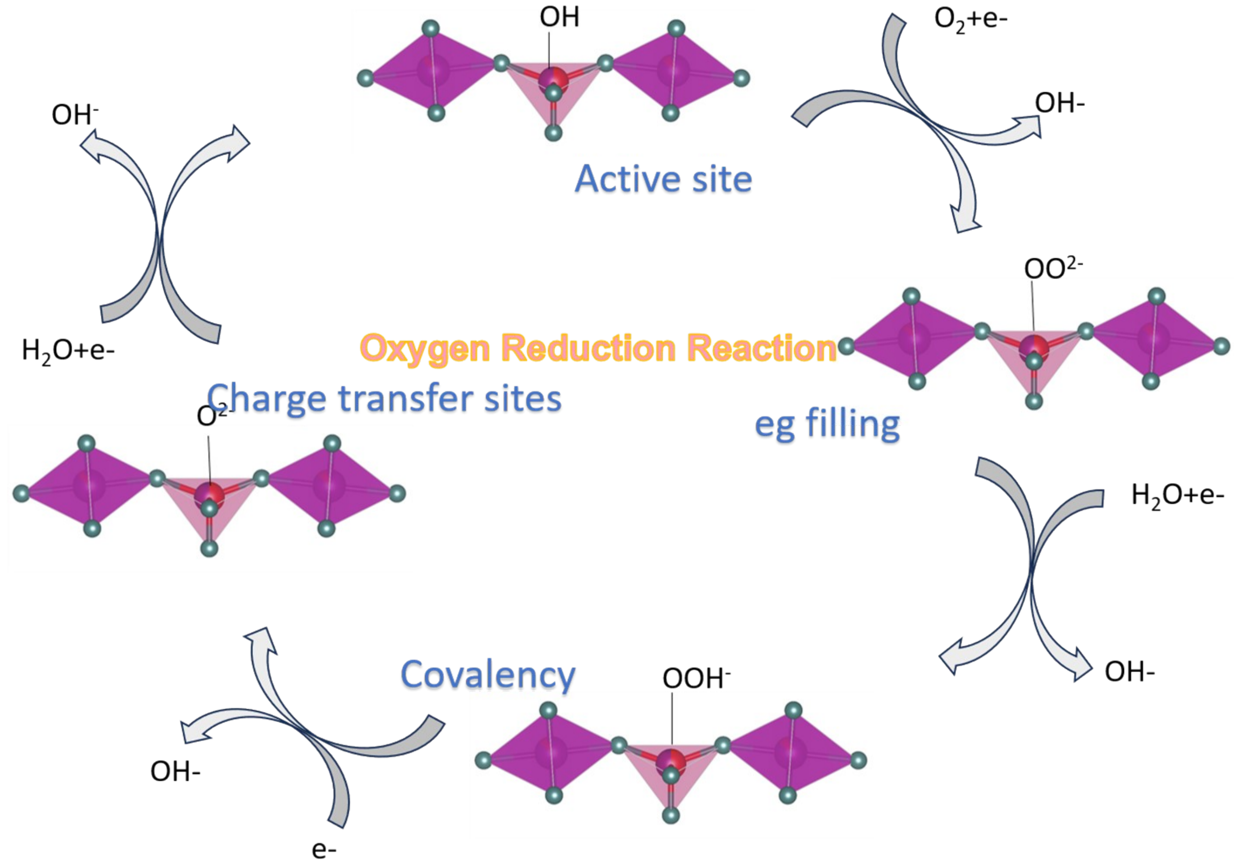

Figure S18: A possible ORR mechanism for Sr_2MnFeO_5 perovskite oxide

S19: e_g electron calculation

The average e_g electron can be calculated from the equation (3) in the main manuscript. For example,

$SrMn_{0.7}Fe_{0.3}O_3$, the percentage of valence electron

n = -1/2 [0*0.58.8+1*0.69+1*0.34+2*0.61] = 1.12

Sr_2MnFeO_5 The percentage of valence electron

n= -1/2 [1*0.49+ 2* 66.9 +1* 32.9] =1.0

Table S1: Reflection planes of (a) $SrMn_{0.8}Fe_{0.2}O_3$, (b) $SrMn_{0.7}Fe_{0.3}O_3$, and (c) Sr_2MnFeO_5

a)

2 Theta	hkl
22.78	012
22.84	012
32.35	110
32.4	110
32.5	104
32.61	104
38.22	113
38.32	113
39.9	202
40.23	006
40.34	006
46.54	024
46.66	024
50.86	211
51.00	211
52.31	122
52.45	122
52.54	116
52.68	116
57.71	300
57.82	214
57.87	018
57.98	018
58.15	125
61.74	220
67.73	208
67.92	131
68.14	223
68.33	134
71.30	134
71.35	223
77.17	134
77.40	134
77.46	128
80.63	315
81.63	042
81.82	226

b)

2 Theta	
16.94	
22.6	
22.74	
22.79	
23.31	
25.44	
25.50	
32.17	
32.29	
32.58	
32.71	
34.27	
34.22	
34.19	
34.22	
34.27	
34.31	
34.57	
34.66	
36.65	
36.7	
36.9	
37.02	
39.69	
43.45	
46.19	
46.44	
46.62	
46.84	
47.68	
46.80	
47.95	
47.97	
48.07	
49.62	
57.41	
57.44	
57.67	
57.71	
57.95	
58.94	
67.31	
68.70	
77.73	

c)

2 Theta	hkl
22.85	012
32.48	110
32.61	104
38.35	113
40.09	202
40.30	006
46.69	024
51.07	211
52.52	122
52.68	116
57.96	300
58.03	214
58.11	300
58.19	214
58.27	018
61.96	125
68.03	220
68.32	208
71.62	131
71.65	223
71.82	131
71.83	217
71.86	223
71.97	119
72.03	217
72.17	119
72.81	312
72.95	036
73.02	312
73.16	036
77.50	134
77.70	128
77.73	134
80.96	315
82.01	042

Table S2: Summary of refined cell parameters of $SrMnO_3$, $SrMn_{0.8}Fe_{0.2}O_3$, $SrMn_{0.7}Fe_{0.3}O_3$, $SrMn_{0.5}Fe_{0.5}O_3$ and Sr_2MnFeO_5

Sample	Crystal System	Space Group & No	Lattice Cell (Å)	Cell Volume	Fit Parameter
$SrMnO_3$	Hexagonal	P63/mmc & 194	a= 5.4484 b= 5.4484 c= 9.0865	233.6	R_p: 779 $R_{wp:}$ 48.5 Chi Square:1.5
$SrMn_{0.8}Fe_{0.2}O_3$	Trigonal	R-3C &167	a=5.5289 b=5.5289 c=13.4367	355.7	R_p: 97.1 R_{wp}: 56.6 R_e: 35.6 Chi Square: 2.5
$SrMn_{0.7}Fe_{0.3}O_3$	Trigonal	R-3C &167	a= 5.5067 b= 5.5067 c= 13.4142	352.2	R_p: 119 R_{wp}: 65.8 R_e: 8.9 Chi Square: 2.7
$SrMn_{0.5}Fe_{0.5}O_3$	Trigonal	R-3C &167	a= 5.5075 b= 5.5075 c= 13.4167	352.4	R_p: 127 R_{wp}: 60 R_e:41.7 Chi Square: 2.1
Sr_2MnFeO_5	Orthorhombic	Icmm & 74	a=5.5591 b=15.7079 c=5.4918	479.5	R_p:177 R_{wp}: 72 R_e: 48.5 Chi Square: 2.2

R_p: Residual parameter, R_{wp}: Residual weight parameter, and R_e: Expected reliable factor

Table S3: Area integrated Manganese and iron contents for $SrMn_{0.7}Fe_{0.3}O_3$ and Sr_2MnFeO_5 obtained from XPS

Composition (%)	**Mn^{4+}**	**Mn^{3+}**	**Mn^{2+}**	**Fe^{3+}**	**Fe^{2+}**	**Fe^0**
$SrMn_{0.7}Fe_{0.3}O_3$	58.8	40.2	-	61.2	38.7	
Sr_2MnFeO_5	20.3	62.5	17.2	57	30	11

Table S4: Summary of ORR electrochemical data (onset and halfwave potential, limiting currrent density and the number of electrons transferred) for all the synthesized catalysts **supported on carbon**

Electrocatalyst	E_{onset} (V); vs RHE	$E_{1/2}$ (V); vs RHE	Current density (mA cm^{-2})	Chronoamperometry Retention Current (%)
$SrMn_{0.8}$ $Fe_{0.2}$ O_3	0.95	0.78	5.0	54
$SrMn_{0.7}$ $Fe_{0.3}$ O_3	0.99	0.84	6.3	95.8
$SrMn_{0.5}Fe_{0.5}O_3$	0.95	0.77	4.9	90.6
Sr_2MnFeO_5	0.89	0.71	5.4	85

Table S5: Summary of ORR electrochemical data (onset and halfwave potential, limiting currrent density and the no. of electrons transferred) for all the synthesized catalysts **without carbon support**.

Electrocatalyst	E_{onset} (V); vs RHE	$E_{1/2}$ (V); vs RHE	Current density (mA cm^{-2})
$SrMn_{0.7}Fe_{0.3}O_3$	0.89	0.68	1.71
$SrMn_{0.8}Fe_{0.2}O_3$	0.92	0.76	2.46
$SrMn_{0.5}Fe_{0.5}O_3$	0.90	0.76	2.31
Sr_2MnFeO_5	0.97	0.78	2.4

Table S6: Bond distance length in (Å),Mn-O, Fe-O, Mn-O-Mn, Mn-O-Fe and Mn-Fe as observed in $SrMn_{0.8}Fe_{0.2}O_3$, $SrMn_{0.7}Fe_{0.3}O_3$, $SrMn_{0.5}Fe_{0.5}O_3$ and Sr_2MnFeO_5.

Composition	Mn-O(1) (Å)	Fe-O(2) (Å)	Mn-O(1)-Mn (Å)	Mn-O(2)-Fe (Å)	Mn-Fe (Å)
$SrMn_{0.8}Fe_{0.2}O_3$	1.97172	1.97172	1.97172	1.97172	-
$SrMn_{0.7}Fe_{0.3}O_3$	2.00497	2.00497	2.00497	2.00497	-
$SrMn_{0.5}Fe_{0.5}O_3$	1.95406	1.95406	1.95406	1.95406	-
Sr_2MnFeO_5	1.95586	1.95586	1.84502	1.84502	0.42396

Table S7: O1–O1 bond distance length in (Å), O-Mn-O and O–Mn–O bond angle (°) as Observed in $SrMn_{0.8}Fe_{0.2}O_3$, $SrMn_{0.7}Fe_{0.3}O_3$, $SrMn_{0.8}Fe_{0.2}O_3$ and Sr_2MnFeO_5.

Composition	O1-O1 (Å)	O-Mn-O (°) Face sharing	Mn-O-Mn (°) Corner sharing	Fe-O-Fe (°) Corner sharing	Mn-O-Fe (°)
$SrMn_{0.8}Fe_{0.2}O_3$	2.81100	89.0692	162.841	162.841	162.841
$SrMn_{0.7}Fe_{0.3}O_3$	2.78689	90.9313	151.8	151.8	151.8
$SrMn_{0.5}Fe_{0.5}O_3$	2.7757	90.5118	168.158	168.158	168.158
Sr_2MnFeO_5	2.74383	78.2867	137.921	138.3	138.376

Table S8: ECSA, Mass activity and Specific activity listed for all the synthesized catalysts.

Electrocatalyst	ECSA (m^2g^{-1})	Mass Activity ($mA\ mg^{-1}$)	Specific Activity ($mA\ cm^{-2}$)
$SrMn_{0.8}Fe_{0.2}O_3$	1.8	35.4	1.91
$SrMn_{0.7}Fe_{0.3}O_3$	8.2	121.3	1.47
$SrMn_{0.5}Fe_{0.5}O_3$	5.4	41.8	0.76
Sr_2MnFeO_5	1.5	24.8	1.56

Table S9: Summary of the literature reports for ORR and OER

Electrocatalyst	Loading ($mg\ cm^{-2}$)	$E_{onset=}$ (V; vs RHE)	Current density J($mAcm^{-2}$)	$E_{1/2(ORR)}$ (V; vs RHE)	$E_{j-10\ (OER)}$ (V; vs RHE)	$\Delta E=E_{j-10(OER)}-E_{1/2(ORR)}$ (V; vs RHE)	Ref
$SrMn_{0.7}Fe_{0.3}O_3$	0.28	0.99	6.38	0.84	1.66	0.82	This work
$SrMn_{0.5}Fe_{0.5}O_3$	0.28	0.95	4.87	0.77	1.79	1.01	This work
$SrMn_{0.8}Fe_{0.2}O_3$	0.28	0.95	5.01	0.78	-	-	This work
Sr_2MnFeO_5	0.28	0.89	5.4	0.71	1.82	0.93	
LaFeCo-H		0.750	5.2	0.713			
$La_{23/}Sr_{1/3}MnO_3$	0.5	0.87	-	0.8	-	-	4
$LaMnO_3$	0.312			0.67	1.80	1.13	1
$LaMn_{0.4}Co_{0.6}O_3$	0.312			0.71	1.63	0.92	1
$LaMn_{0.2}Co_{0.8}O_3$	0.312			0.68	1.64	0.96	1
$La_{0.8}Sr_{0.2}Mn_{1-x}Ni_xO_3$	NA	0.74	-	-	1.54 @ 2mA cm^{-2}	-	3
$La_{0.4}Sr_{0.6}MnO_3$	0.5	-0.197 vs SCE (V)	-4.54	-	0.774 @ 5 mA cm^{-2}	0.97	2
MnO[illegible]/La[illegible]Sr[illegible]MnO[illegible]							5

	0.47	0.87		0.75	1.727	0.89	
$Sr_4Mn_3O_{10}$	NA	0.80	-	0.5	-	-	6
$La_{0.9}Y_{0.1}MnO_3$	0.236	0.90	6.58	0.75	1.8	-	7
$LKMnO_3$	NA	-	-	0.78	1.66	-	8
$La_{0.6}Ca_{0.4}CoO_3$/Sb doped SnO_2	NA	0.76	2.8	0.79	1.60	-	9
$A_xSm_{1-x}Mn_2O_{5-\delta}(Ba_xSn_{1-x}Mn_2O_{5-\delta})$	0.25	0.884		0.789			10
$La_{0.85}Y_{0.15}Ni_{0.7}Fe_{0.3}O_3$	0.2	0.71	-3.7	0.62	1.63 @ 10 mA		11
$La_2Co_{0.5}Fe_{0.5}MnO_{6-\delta}$	NA	0.78	-6.1	0.62	1.65		12
$LaCoO_3$ @ rGO	NA	0.85	-5.5	0.70	1.51 @280 mV		13
$La_{0.8}Sr_{0.2}Ti_{0.65}Fe_{0.35}O_{3-\delta}$ LSTFO/NCNT	1.0	0.992	6.07	0.86	1.77	0.76	14

References

1. Jiang, X., Dong, Y., Zhang, Z., Li, J., Qian, J., & Gao, D.. Cation substitution of B-site in $LaCoO_3$ for bifunctional oxygen electrocatalytic activities. *Journal of Alloys and Compounds*, **2021**, 878, 160433.

2. Zhao, Y., Hang, Y., Zhang, Y., Wang, Z., Yao, Y., He, X.,& Zhang, D. Strontium-doped perovskite oxide $La_{1-x}Sr_xMnO_3$ (x= 0, 0.2, 0.6) as a highly efficient

electrocatalyst for nonaqueous Li-O_2 batteries. *Electrochimica Acta*,**2017**, 232, 296-302.

3. Islam, M., Jeong, M. G., Oh, I. H., Nam, K. W., & Jung, H. G. Role of strontium as doping agent in $LaMn_{0.5}Ni_{0.5}O_3$ for oxygen electro-catalysis. *Journal of Industrial and Engineering Chemistry*, **2020**, 85, 94-101.

4. Eom, C. J., Kuo, D. Y., Adamo, C., Moon, E. J., May, S. J., Crumlin, E. J.,& Suntivich, J. Tailoring manganese oxide with atomic precision to increase surface site availability for oxygen reduction catalysis. *Nature communications*,**2018**, 9(1), 1-7.

5. Yan, S., Xue, Y., Li, S., Shao, G., & Liu, Z. Enhanced bifunctional catalytic activity of manganese oxide/perovskite hierarchical core–shell materials by adjusting the interface for metal–air batteries. *ACS applied materials & interfaces*,**2019**, 11(29), 25870-25881.

6.González-Jiménez, I. N., Torres-Pardo, A., Rano, S., Laberty-Robert, C., Hernández-Garrido, J. C., López-Haro, M.,& Portehault, D. Multicationic $Sr_4Mn_3O_{10}$ mesostructures: molten salt synthesis, analytical electron microscopy study and reactivity. *Materials Horizons*, **2018**,5(3), 480-485.

7. Miao, H., Wang, Z., Wang, Q., Sun, S., Xue, Y., Wang, F., & Yuan, J. A new family of Mn-based perovskite ($La_{1-x}Y_xMnO_3$) with improved oxygen electrocatalytic activity for metal-air batteries. *Energy*, **2018**,154, 561-570.

8. Kotha, V., Karajagi, I., Ghosh, P. C., & Panchakarla, L. S. Potassium-Substituted $LaMnO_3$ as a Highly Active and Exceptionally Stable Electrocatalyst toward Bifunctional Oxygen Reduction and Oxygen Evolution Reactions. *ACS Applied Energy Materials*, **2022**

9. Fujiwara, Naoko, Tsukasa Nagai, Tsutomu Ioroi, Hajime Arai, and Zempachi Ogumi. "Bifunctional electrocatalysts of lanthanum-based perovskite oxide with Sb-

doped SnO2 for oxygen reduction and evolution reactions." *Journal of Power Sources,* **2020,** 451,227736.

10. Zhao, Chunning, Meng Yu, Zhi Yang, Jieyu Liu, Shaohua Chen, Zhanglian Hong, Haijun Chen, and Weichao Wang. "Oxygen reduction reaction catalytic activity enhancement over mullite $SmMn_2O_5$ via interfacing with perovskite oxides." *Nano Energy,* **2018**, 51: 91-101.

11. X. Wang, J. Sui, Z. Hou, M. Zhang, Q. Zhang, J. Yu, Z. Gan, L. Sui, L. Dong. "LSCF perovskite oxide in situ grown on reduced graphene oxide as high-performance bifunctional catalyst for zinc-air battery." *Diamond and Related Materials,* **2023**, 132,: 109668.

12. L. Fengjiao, N. Mushtaq, T. Su, Y. Cui, J. Huang, M. Sun, M. Singh. "NCNT grafted perovskite oxide as an active bifunctional electrocatalyst for rechargeable zinc-air battery." *Materials Today Nano.* **2023**, 21, 100287.

13.Y. Chunyang, Y. Gan, M. Lee, C. Ren, K. S. Brinkman, R. D. Green, X. Xue. Structural evolution, electrochemical kinetic properties, and stability of A-site doped perovskite $Sr_{1-x}Yb_xCoO_{3-\delta}$. *Journal of Materials Chemistry A*. **2020**, 8, no. 20, 10450-10461. (A- site)

14. A. Jahangeer, T. Ahamad, N. Alhokbany, MA Majeed Khan, Prabhakarn Arunachalam, Mabrook S. Amer, Rahaf M. Alotaibi, and Saad M. Alshehri. "Reduced graphene oxide encapsulated perovskite-type lanthanum cobalt oxide nanoparticles for efficient electrolysis of water to oxygen reactions (OER/ORR)." *Journal of Industrial and Engineering Chemistry* **2023**.